Adaptive Partial Median Filter for Early CT Signs of Acute Cerebral Infarction

Yongbum Lee, Noriyuki Takahashi*, Du-Yih Tsai and Kiyoshi Ishii*

Dept. of Radiological Technology, School of Health Sciences, Niigata Univ., 2-746 Asahimachidori, Niigata, 951-8518 Japan

**Dept. of Radiology, Sendai City Hospital, 3-1 Simizukouji Wakabayasi, Sendai, 984-0075 Japan*

Phone: +81-25-227-0957

FAX: +81-25-227-0749

Email: lee@clg.niigata-u.ac.jp

Abstract:

Purpose: Detection of early CT signs of infarct in non-enhanced CT image is mandatory in patients with acute ischemic stroke. Loss of the gray-white matter interface at the lentiform nucleus or the insular ribbon has been an important early CT sign of acute cerebral infarction, which affects decisions on thrombolytic therapy. However, its detection is difficult, since the principal early CT sign is subtle hypoattenuation. An image processing method to reduce local noise with edges preserved was developed to improve infarct detection.

Rationale: An adaptive partial median filter (APMF) was selected for this application, since the APMF can markedly improve the visibility of the normal gray-white matter interface. APMF should enhance the conspicuity of gray-white matter interface changes due to hypoattenuation that accompanies cerebral infarction.

Method: In a criterion referenced performance study using simulated CT images with gray-white matter interfaces, a total of 14 conventional smoothing filters were also used for comparison to validate the usefulness of the proposed APMF. The APMF indicated the highest performance among the compared methods. Then, observer performance study by receiver operator characteristic (ROC) analysis was performed with 4 radiologist observers using a database with 18 abnormal and 33 normal head CT images.

Results: The average A_z values of ROC curves for all radiologists increased from 0.876 without the APMF images to 0.926 with the APMF images, and this difference was statistically significant (P=0.04).

Conclusion: The results from the two observer performance studies demonstrated that APMF has significant potential to improve the diagnosis of acute cerebral infarction using non-enhanced CT images.

Keyword: computer-aided diagnosis (CAD), acute cerebral infarction, noise reduction, edge preserving, improved median filter

I. INTRODUCTION

The mortality rate for cerebrovascular disease is approximately ten percents in all deaths in the world [1]. The cerebrovascular disease is a major cause of disability and is one of the three leading causes of death with heart disease and malignant neoplasm in several countries, e.g. Japan [2]. Acute cerebral infarction is one of the major cerebrovascular disease, and detection of its early signs is very important for survival and convalescence. Currently, computer tomography (CT) is still the most commonly used imaging modality in the diagnosis of acute cerebral infarction because of its wide availability and examination speed,

though the advanced magnetic resonance (MR) imaging is superior to the non-enhanced CT in respect of sensitivity in the detection of cerebral ischemia within the first few hours after symptom onset [3],[4]. With the introduction of thrombolysis, much attention has been directed to identify early CT signs, which are subtle early signs of ischemic changes on CT images, over the last decade [5]-[7]. Detection of early CT signs is of importance in middle cerebral artery (MCA) strokes within the first few hours of the onset of symptoms. One of the notable early CT signs is the loss of gray-white matter interface, e.g. lenticular nuclei, due to the hypoattenuating appearance of gray matter structures [8],[9]. However, because of the subtle appearance of the loss of gray-white matter interface resulting from image noise, the radiologists may not be able to visually identify it [10],[11].

Recently technological innovation of CT units has dramatically advanced, so that image noise originated by the CT unit itself can be negligible. However, quantum noise due to X-ray quanta registered by the image detector cannot be prevented, even though using an ideal CT unit [12]. The quantum noise degrades the visibility of low-contrast structures such as normal gray-white matter interface on CT images. Under this condition, one can hardly recognize the normal gray-white matter interface on CT images, much less the loss of the gray-white matter interface due to cerebral ischemia. To solve this problem, it is necessary to improve the visibility of normal gray-white matter interface by removing or reducing the quantum noise with any ways. High-dose CT, for example, can reduce the quantum noise. However, this results in increasing patient radiation exposure. Hence, image processing techniques may become appropriate ways to reduce the quantum noise and consequently to improve the visibility of normal gray-white matter interface on CT images. Although various advanced digital filters for reducing image noise on CT images have been reported. However, these filters were mainly designed to deal with the reduction of radiation dose [13], [14]. In the present study, we focused on directly improving the visibility of normal gray-white matter interface on non-enhanced CT images by using a noise reduction filter. We believe that if noise is reduced, then the normal gray-white matter interface can be relatively enhanced. As a result, the loss of gray-white matter interface due to stroke could be more detectable. An exclusive smoothing filter is desirable to eliminate the quantum noise with almost no blurring of the edge of gray-white matter interface. To overcome this issue, an adaptive partial median filter (APMF) was proposed in this paper. The algorithm of APMF refers to Guis's contrast enhancement method [15] and is based on adaptive partial averaging filter (APAF) previously reported [16],[17]. The distinction between APAF and APMF is simply the difference between "*averaging*" and "*median*" in a step of procedure. The APMF has a characteristic: noise can be reduced without degrading signal, i.e., edge. In the field of image processing, various image filtering techniques for noise reduction have been reported [18]-[33], and almost of them were edge-preserving smoothing techniques. In our previous work [16],[17], only two conventional filters, which were averaging filter and median filter, were used to compare with APAF, and no observer performance study was made. In this paper, first, APMF was compared to 14

conventional smoothing techniques by criterion-referenced performance study. Simulated CT images with gray-white matter interfaces were used for the study. Next, APMF was applied to a clinical database for application to actual clinical cases for preliminary observer performance study. Its usefulness was evaluated by receiver operator characteristic (ROC) analysis. Details of them will be described in each section in order.

II. APATIVE PARTIAL MEDIAN FILTER

The APMF is a specially designed filter with local median processing using a variable filter size and shape. The APMF's main steps are as follows, and illustrations corresponding to each step of APMF procedure are shown in Fig.1.

Step 1: An averaging filter with $M \times M$ mask size is applied to the original image.

Step 2: A window image whose initial size is $W_{max} \times W_{max}$ is assigned from the original image after the averaging filter. W_{max} is a positive odd number from 3.

Step 3: A mask image is generated by assigning a binary mask value 0 if $|I(i, j)-I(i_c, j_c)|>T$, and by assigning a binary mask value 1 if $|I(i, j)-I(i_c, j_c)|\leq T$. $I(i_c, j_c)$ and $I(i, j)$ are defined as the pixel value of the center pixel and the pixel value of an arbitrary pixel in the window image, respectively.

Step 4: For each window size $W \times W$ [W=3,5,…., W_{max}], the percentage P_0 of 0 in the mask image is computed over the region of external area of each window image. Actual window size is determined when the percentage P_0 is not greater than P%, and is closest to P%.

Step 5: Finally, a median value is obtained from the pixel values $I(i, j)$ corresponding with mask value 1 in mask image, and the median value is used as output value at the center pixel value $I(i_c, j_c)$.

Step 6: Steps 2~5 are performed at each pixel.

Step 1 is related to differentiating between the object pixel value $I(i_c, j_c)$ and the surrounding pixel value $I(i, j)$ described in Step 3. As noise superimposed on the object pixel has to be initially reduced, otherwise the APMF will not perform well. Step 3 is based on an assumption that variation of pixel values due to noise is smaller than the difference of pixel values due to signal, and is an important process to distinguish between noise and signal components. In Step 4, actual window size will be small to enhance the quality of edge preserving if there are many pixels with pixel values larger than T in window image. In contrast, the actual window size will be large to enhance the noise reduction rate if pixel values in window image are almost uniform. As for APAF[16],[17], "*median*" is just replaced to "*averaging*" in Step 5.

The performance of the APMF depends on parameters M, W_{max}, T and P. In particular, T is very important parameter because it determines rough boundary of object, e.g. lenticular nuclei on a CT image. T distinguishes object region (mask value 1) and background region (mask value 0). Then only pixel values in object region are used for computation. It means

that the APMF is able to reduce local noise while preserving edge components between object and background regions. Therefore, T for application to clinical images was obtained by a simulation study described in the next section. The other parameters of M=5, W_{max}=13, and P=60 were determined using the rule of trial and error on simulated images to be described in the next section.

III. CRITERION-REFERENCED PERFORMANCE STUDY

A. Materials

Our simulation study has two purposes. One is to determine an adequate parameter of T for application to clinical CT images. The other one is to validate the superiority of the APMF by comparing with conventional smoothing techniques. Composite images with simulated white matter (SWM) and simulated gray matter (SGM) were used for this simulation. First, in order to obtain the simulated SWM, cylindrical phantom which was Catphan CT phantom CTP486 made by The Phantom Laboratories, Inc. was scanned by CT device which was Somatom Volume Zoom made by Siemens-Asahi Medical Technologies Ltd.. Then, the SGM was put on the CT image. Concretely, 3~6HU (Hounsfield Unit) was added to the SWM by computation because the contrast of normal gray-white matter interface was approximately 6HU, and the contrast of ischemic gray-white matter interface deteriorated to approximately 3HU. Fig.2 shows a simulation image and its sketch. The size of simulation image shown in Fig.2 is 300×300 pixels. This is a part of original image whose size is 512×512 pixels. Edge slope between SWM and SGM on the dotted line in sketch of Fig.2 has been generated as shown in Fig.3. C_x in Fig.3 corresponds to the abscissa of the dotted line in sketch of Fig.2. The *cnt* in Fig.3 corresponds to the contrast between SWM and SWM, which is 3~6HU. The CT scan specifications were Tube Voltage 120kV, Tube Current 200~400mAs, Slice Thickness 10mm, FOV (field of view) 250mm, and matrix size 512×512. The phantom was scanned ten times under the same condition, and then ten composite images were generated under the same condition to restrain variation of evaluation values that will be described in the next paragraph. The total number of simulation images was 120 which was obtained by 4 contrast levels (3~6HU, interval of 1 HU) × 3 noise levels (200~400mAs, interval of 100mAs) × 10 scans.

B. Criteria

The standard deviation rate (*SDR*) and edge slope rate (*ESR*) were used as two criteria for measuring the performance of the APMF and the conventional smoothing techniques. The standard deviation of the pixel values in a specified area, which was used to quantify the degree of noise reduction, was obtained from a region of 20×20 pixels on the SGM, as shown in Fig.2. To investigate the extent of edge preserving, edge slope rate was calculated from an average profile of pixel values, which was measured at the horizontal direction with respect to the edge on the dotted line shown in Fig.2. The standard deviation rate was computed by

$$SDR(\%) = \left(SD_{org} - SD_{prc}\right) \Big/ SD_{org} \times 100 .$$

SD_{org} is an average standard deviation calculated from ten original composite images, and SD_{prc} is an average standard deviation calculated from ten processed images. The edge slope rate was computed by

$$ESR(\%) = ES_{prc} \big/ ES_{org} \times 100$$

where $ES_{prc} = \left\{V_{prc}(c_x) - V_{prc}(c_x - 3)\right\}\big/3$,

$ES_{org} = \left\{V_{org}(c_x) - V_{org}(c_x - 3)\right\}\big/3$ as shown in Fig.3.

ES_{org} is an average edge slope value calculated from ten original composite images, and ES_{prc} is an average edge slope value calculated from ten processed images. High *SDR* means that the noise is decreased well. High *ESR* means that the edge is highly preserved.

C. Performance comparison

The APMF was compared to 14 conventional smoothing filters, namely, averaging filter (AF) [18], median filter (MF) [19], gaussian filter (GF) [18], k-nearest neighbor averaging (KNNA) [20], k-nearest neighbor median (KNNM) [21], hysteresis smoothing (HS) [22], edge and line weights smoothing (ELWS) [23], contrast sensitive weights smoothing (CSWS) [23], gradient inverse weighted smoothing (GIWS) [24], Nagao's edge preserving smoothing (EPS) [25], adaptive rank order filter (AROF) [26], adaptive two pass median filter (ATPMF) [27], adaptive noise smoothing filter (ANSF) [28], and adaptive partial averaging filter (APAF) [16],[17] which was a basis of APMF. The *SDR* and *ESR* of each method were calculated from the processed composite images obtained by varying Tube Current (200, 300, 400mAs) and the contrast (3, 4, 5, 6HU) between SGM and SWM. As a sample of results, Fig.4 shows graphs of *SDR* and *ESR* in the case of 400mAs, 6HU. For those methods with variable filter size (*FS*), namely, AF, MF, GF, KNNA, KNNM, AROF, ATPMF and ANSF, the filter size was used as variable of the horizontal axis on the graphs. This means that *SDR* and *ESR* were calculated by varying filter size. For those methods with fixed filter size, namely, ELWS, CSWS, GIWS, and EPS, the number of iteration (*NI*) was used as variable of the horizontal axis on the graphs. This means that *SDR* and *ESR* were calculated by varying the number of iteration. HS has an only parameter of *Width* which is an established hysteresis cursor size, and is at least equal to the size of the largest waveform peak or valley to be removed [22]. Therefore, the *Width* was used as variable of the horizontal axis on the graph of HS. The parameters of APAF are the same with the parameters of APMF because the difference between APAF and APMF is only whether the output value at the center pixel value $I(i_c, j_c)$ in Step 5 in Section II is the averaging value or the median value [16],[17]. Therefore, the parameter *T* was used as variable of the horizontal axis on the graph of APAF, as that of APMF. Other parameters as shown in Table 1, which were σ of GF and CSWS, *a* and *b* of ATPMF, and *k* of KNNA and KNNM, were determined experimentally by referring to the respective literatures.

Table 1 shows specific values of *SDR* and *ESR* extracted from the graphs in Fig.4. The specific values were based on *SDR* and *ESR* of APMF at *T*=3. We supposed that *T*=3 was the

best value of *T* because *ESR* at *T*=3 was highest, and *SDR* at *T*=3 was almost highest. The details of this topic will be described in the next paragraph. In regard to AF, MF, GF, ELWS, CSWS, ATPMF, ANSF and APAF, the values of *ESR* were selected out when the values of *SDR* became most closest to the *SDR* (76.0%) of APMF. In regard to the others which were KNNA, KNNM, HS, AROF, GIWS and ESP, the values of *SDR* were selected out when the values of *ESR* became most closest to the *ESR* (71.7%) of APMF because the values of *SDR* did not become close to the *SDR* of APMF. In Table 1, highest *ESR* was 71.7% of APMF at the almost same *SDR*, and then in order, it was 64.0% of APAF, 51.4% of ELWS, and 49.9% of ATPMF. The *ESR* of the others, which were AF, MF, GF and CSWS, were less than 34.0%. In comparison in a condition of almost same *ESR*, highest *SDR* was 76.0% of APMF, and then the *SDR* of the others, which were KNNA, KNNM, HS, AROF, GIWS and EPS, were less than 55.0%. The processed images by each method with parameters shown in Table 1 are shown in Fig.5. These are parts of processed images around SGM-SWM interface. The image qualities are well consistent with the criterion values shown in Table 1. These comparison results clearly indicated that the APMF had the highest performance among the compared methods. The all results in conditions by varying Tube Current (200, 300, 400mAs) and the contrast (3, 4, 5, 6HU) between SGM and SWM had the same tendencies.

D. Adequate T for clinical images

Clinical brain CT images used in this study were scanned by the ProSeed Accell made by GE Yokogawa Medical System, whose specifications were Tube Voltage 120kV, Tube Current 400mAs, Slice Thickness 10mm, FOV 250mm, and matrix size 512×512. These specifications corresponds to those for sample graph of APMF shown in Fig.4. Therefore, an adequate *T* could be determined by referring to the simulation result of APMF as shown in Fig.4. *SDR* almost stop increasing from *T*>3, and *ESR* began to decrease sharply from *T*>3 (the peak at *T*=3). Fig.7 shows the processed images obtained by varying the threshold value *T* [0, 1, 2, 3, 4, 5, 6] of APMF. The APMF image at *T*=3 looks very well with regard to edge sharpness and noise reduction. The APMF images at *T*=0, 1, 2 are insufficient on the degree of noise reduction, and the APMF images at *T*=4, 5, 6 are too blurry. Considering these data, *T*=3 might be an adequate threshold value in the condition of 400mAs and on the assumption that the contrast of gray-white matter interface on clinical brain CT image was approximately 6HU. Therefore, *T*=3 was determined as an adequate parameter for applying to clinical CT images in this study.

IV. PRELIMINARY OBSERVER PERFORMANCE STUDY

The APMF at *T*=3 was applied to 51 non-enhanced brain CT images which consisted of 18 abnormal images and 33 normal images, and then observer study with ROC analysis was performed by 4 radiologists. The abnormal images were obtained from 18 patients (mean age, 74 years) with acute (within 5 hours) cerebral infarction, and all of them showed subtle loss of the gray-white matter interface in the cortical ribbon and/or in the lentiform nucleus. The

normal images were obtained from 33 control patients (mean age, 68 years). Two samples of abnormal cases used in this study are shown in Fig.8. A sample supplies three CT images, which are original image, APMF image and follow-up image obtained several days after the onset of symptoms. The original image of case 1 illustrated on the upper left in Fig.8 was obtained in a 83-year-old-female with right hemiplegia at 2.4 hours after stroke onset. The APMF image shows that the loss of the gray-white matter interface at the left lentiform nucleus, the so-called obscured outline of the lentiform nucleus, is clearly detectable (arrows). The outline of the right normal lentiform nucleus is obviously visible compared to the corresponding contralateral one. The follow-up image demonstrates infarction in the left middle cerebral artery (MCA) and anterior cerebral artery (ACA) distributions. The original image of case 2 illustrated on the lower left in Fig.8 was obtained in a 83-year-old-male with right hemiplegia at 1.5 hours after stroke onset. The APMF image shows that the loss of the gray-white matter interface of posterior part of the left lentiform nucleus is clearly detectable. The follow-up image demonstrates infarction in the left middle cerebral artery (MCA) and posterior cerebral artery (PCA) distributions. Two samples vividly indicated that early CT signs of acute cerebral infarction were remarkably enhanced in the APMF images.

Four radiologists including two attending radiologists (years of experience, 14-18 years) and two radiology resident (years of experience, 1-3 years) independently interpreted the cases on the monitor for this observer study. First diagnostic decisions of them were determined by interpreting only original images. Window width (WW) and window level (WL) were free in their interpreting. Although there were some reports that diagnostic accuracy would be improved by using narrow WW in interpreting on the monitor [34], narrow WW enhances not only edge such as gray-white matter interface but quantum noise in non-enhanced CT image. Therefore, default WW and WL for original images were 80 and 35HU, respectively, because it was the general condition for diagnosis in radiologist's daily work in Japan. After first interpreting, they could correct their decisions by reinterpreting both original and the APMF images. Default WW and WL for the APMF images were 20 and 35HU, respectively. Narrow WW was used for the APMF images as default condition because quantum noises were sufficiently decreased by APMF. Narrow WW after decreasing noises in the APMF images enhances only edges such as gray-white matter interface. The radiologists indicated their confidence rating regarding the presence or absence of early CT sign on each case. The scale of confidence rating ranged from 0 to 100. A computer program (LABMRMC; Charles E. Metz, University of Chicago) [35] was used for obtaining ROC curves and the statistical significance of the difference between the ROC curves by only original images and by original images with APMF images. The area under the ROC curves plotted in the unit square (A_z) was calculated for each fitted curve. The overall performance is illustrated in Table 2 and Fig.9. Table 2 shows the A_z values without the APMF images and with the APMF images for each radiologist. Fig.9 shows the average ROC curves of four radiologists without the APMF images and with the APMF images. The performance of all observers was

improved when the APMF image was used. The average A_z values for all radiologists increased from 0.876 without the APMF images to 0.926 with the APMF images, and this difference was statistically significant (P=0.04). This preliminary result was obtained by only 4 radiologists. As the number of observers was not insufficient, our preliminary result might not provide a sufficient evidence. However, we believe that this preliminary result is suggesting that the APMF can be an useful technique for diagnosis of acute cerebral infarction in non-enhanced CT images.

V. CONCLUSION

In order to improve the detectability of early CT signs for acute cerebral infarction on non-enhanced CT images, a novel adaptive partial median filter (APMF) was proposed. In a criterion-referenced performance study using simulated CT images with gray-white matter interfaces, the APMF was compared with 11 conventional smoothing methods. Two criteria indicating noise reduction rate and edge preserving rate were used for performance evaluation. Our results showed that the APMF had the highest performance among the compared methods. Moreover, the value of the most important parameter T of APMF was determined in the study for application to clinical images. Then, preliminary observer performance study by ROC analysis was performed using 51 clinical CT images including 18 abnormal images obtained within 5 hours after stroke onset. The average A_z values of ROC curves for all radiologists increased from 0.876 without the APMF images to 0.926 with the APMF images, and this difference was statistically significant (P=0.04). This preliminary result of observer study is suggesting that the APMF can be an useful technique for diagnosis of acute cerebral infarction in non-enhanced CT images. The observer performance study using much more cases and by more observers would be required to more clearly prove the usefulness of APMF to clinical cases in the future. We believe that the results from two performance study demonstrate the usefulness of our APMF.

Acknowledgements

This work was supported in part by Grant for Promotion of Niigata University Research Projects and Grant for Scientific Research of Daiwa Securities Health Foundation.

REFERENCES

[1] (2002) The World Health Report 2002, World Health Organization, 186-191
[2] (2004) Journal of health and welfare statistics, Health and Welfare Statistics Association
[3] H.P. Adams, Jr, R.J. Adams, T. Brott, G.J. del Zoppo, A. Furlan, L.B. Goldstein, et al. (2003) Guidelines for the early management of patients with ischemic stroke: A scientific statement from the Stroke Council of the American Stroke Association. Stroke 34:1056-1083
[4] H. Adams, R. Adams, G. del Zoppo, and L.B. Goldstein (2005) Guidelines for the early management of patients with ischemic stroke: 2005 guidelines update a scientific statement from the Stroke Council of the American Heart Association/American Stroke Association. Stroke 36:916-923
[5] R. von Kummer, K.L. Allen, R. Holle, L. Bozzao, S. Bastianello, C. Manelfe, et al.

(1997) Acute stroke: usefulness of early CT findings before thrombolytic therapy. Radiology 205:327-333
[6] J.M. Wardlaw, P.J. Dorman, S.C. Lewis, and P.A. Sandercock (1999) Can stroke physicians and neuroradiologists identify signs of early cerebral infarction on CT?. J Neurol Neurosurg Psychiatry 67:651-653
[7] P.A. Barber, A.M. Demchuk, J. Zhang, and A.M. Buchan (2000) Validity and reliability of a quantitative computed tomography score in predicting outcome of hyperacute stroke before thrombolytic therapy. ASPECTS Study Group. Alberta Stroke Programme Early CT Score. Lancet 355:1670-1674
[8] N. Tomura, K. Uemura, A. Inugami, H. Fujita, S. Higano, and F. Shishido (1988) Early CT finding in cerebral infarction: obscuration of the lentiform nucleus. Radiology 168:463-467
[9] C.L. Truwit, A.J. Barkovich, A. Gean-Marton, N. Hibri, and D. Norman (1990) Loss of the insular ribbon: another early CT sign of acute middle cerebral artery infarction. Radiology 176:801-806
[10] D.L. Schriger, M. Kalafut, S. Starkman, M. Krueger, and J.L. Saver (1998) Cranial computed tomography interpretation in acute stroke: physician accuracy in determining eligibility for thrombolytic therapy. J Am Med Assoc 279:1293-1297
[11] J.M. Wardlaw and O. Mielke (2005) Early signs of brain infarction at CT: observer reliability and outcome after thrombolytic treatment-systematic review. Radiology 235:444-453
[12] W.A. Kalender (2000) Computed Tomography: Fundamentals, System Technology. Image Quality and Applocations, Munich: Publicis MCD
[13] M.K. Kalra, M.M. Maher, D.V. Sahani, M.A. Blake, P.F. Hahn, G.B. Avinash, et al. (2003) Low-dose CT of the abdomen: evaluation of image improvement with use of noise reduction filters-pilot study. Radiology 228:251-256
[14] M. Kachelriess, O. Watzke, and W.A. Kalender (2001) Generalized multi-dimensional adaptive filtering for conventional and spiral single-slice, multi-slice, and cone-beam CT. Med Phys 28:475-490
[15] V.H. Guis, M. Adel, M. Rasigni, and G. Rasigni (2003) Adaptive neighborhood contrast enhancement in mammographic phantom images. Opt Eng 42:357-366
[16] D.Y. Tsai, N. Takahashi, and Y. Lee (2005) An Adaptive Enhancement Algorithm for CT Brain Images. Proc. of the 2005 IEEE Engineering in Medicine and Biology 27th Annual Conference :paper #124.
[17] Y. Lee, N. Takahashi, D.Y. Tsai, and H. Fujita (2006) Detectability improvement of early sign of acute stroke on brain CT images using an adaptive partial smoothing filter. Proc. of SPIE Medical Imaging 6144:2138-2145
[18] J.C. Russ (1995) The Image Processing Handbook, 2nd ed.. FL: CRC Press, Inc., pp.155-178
[19] J.W. Tukey (1971) Exploratory Data Analysis. Addison Wesley
[20] L.S. Davis and A. Rosenfeld (1978) Noise cleaning by iterated local averaging. IEEE Trans Systems Man and Cybernetics SMC-8:705-710
[21] W.Y. Wu, M.J J. Wang and C.M. Liu (1992) Performance evaluation of some noise reduction methods. Comput Vision Graph and Image Processing 54:134-146
[22] R.W. Ehrich (1978) A symmetric hysteresis smoothing algorithm that preserves principal features. Comput Graph and Image Processing 8:121-126
[23] A. Lev, S. W. Zucker and A. Rosenfeld (1977) Iterative enhancement of noisy images. IEEE Trans. Systems, Man, and Cybernetics SMC-7:435-442
[24] D.C.C. Wang, A.H. Vagnucci, and C.C. Li (1981) Gradient inverse weighted smoothing scheme and the evaluation of its performance. Comput Vision Graph and Image Processing 15:167-181
[25] M. Nagao and T. Matuyama (1978) Edge Preserving smoothing. Comput Graph and Image Processing 9:394-407
[26] P. Zamperoni (1990) Some Adaptive Rank Order Filters for Image Enhancement. Pattern Recognition Letters, 11:81-86
[27] X. Xu, E.L. Miller, D. Chen, and M. Sarhadi (2004) Adaptive Two-Pass Rank Order Filter to Remove Impulse Noise in Highly Corrupted Images. IEEE Trans Image Processing 13(2):238-247
[28] D.T. Kuan, A.A Sawchuk, T.C Strand, and P. Chavel (1985) Adaptive Noise

Smoothing Filter for Images with Signal-Dependant Noise. IEEE Trans Pattern Anal Mach Intel 7(2):165-177
[29] J.A.A Centeno and V. Haertel (1997) An Adaptive Image Enhancement Algorithm. Pattern Recognition 30(7):1183-1189
[30] B. Fischl and E.L. Shwartz (1999) Adaptive Nonlocal Filtering: A Fast Alternative to Anisotropic Diffusion for Image Filtering. IEEE Trans Pattern Anal Mach Intel 21(1):42-48
[31] C.F. Westin, J. Richolt, V. Moharir, and R. Kikinis (2000) Affine Adaptive Filtering of CT Data. Med Image Anal 4(2):161-177
[32] A.M.R. Schilham, B.V. Ginneken, H. Gietema, and M. Prokop (2006) Local Noise Weighted Filtering for Emphysema Scoring of Low-Dose CT Images. IEEE Trans Medical Imaging 25(4):451-463
[33] I. Gijbels, A. Lambert, and P. Qiu (2006) Edge-Preserving Image Denoising and Estimation of Discontinuous Surfaces. IEEE Trans Pattern Anal Mach Intel 28(7):1075-1087
[34] M.H. Lev, J. Farkas, J.J. Gemmete, S.T. Hossain, G.J. Hunter, W.J. Koroshetz, and R.G. Gonzalez (1999) Acute stroke: improved nonenhanced CT detection-benefits of soft-copy interpretation by using variable window width and center level settings. Radiology 213:150-155
[35] D.D. Dolfman, K.S. Berbaum, and C.E. Metz (1992) ROC rating analysis: generalization to the population of readers and cases with the jackknife method. Invest Radiol 27:723–731

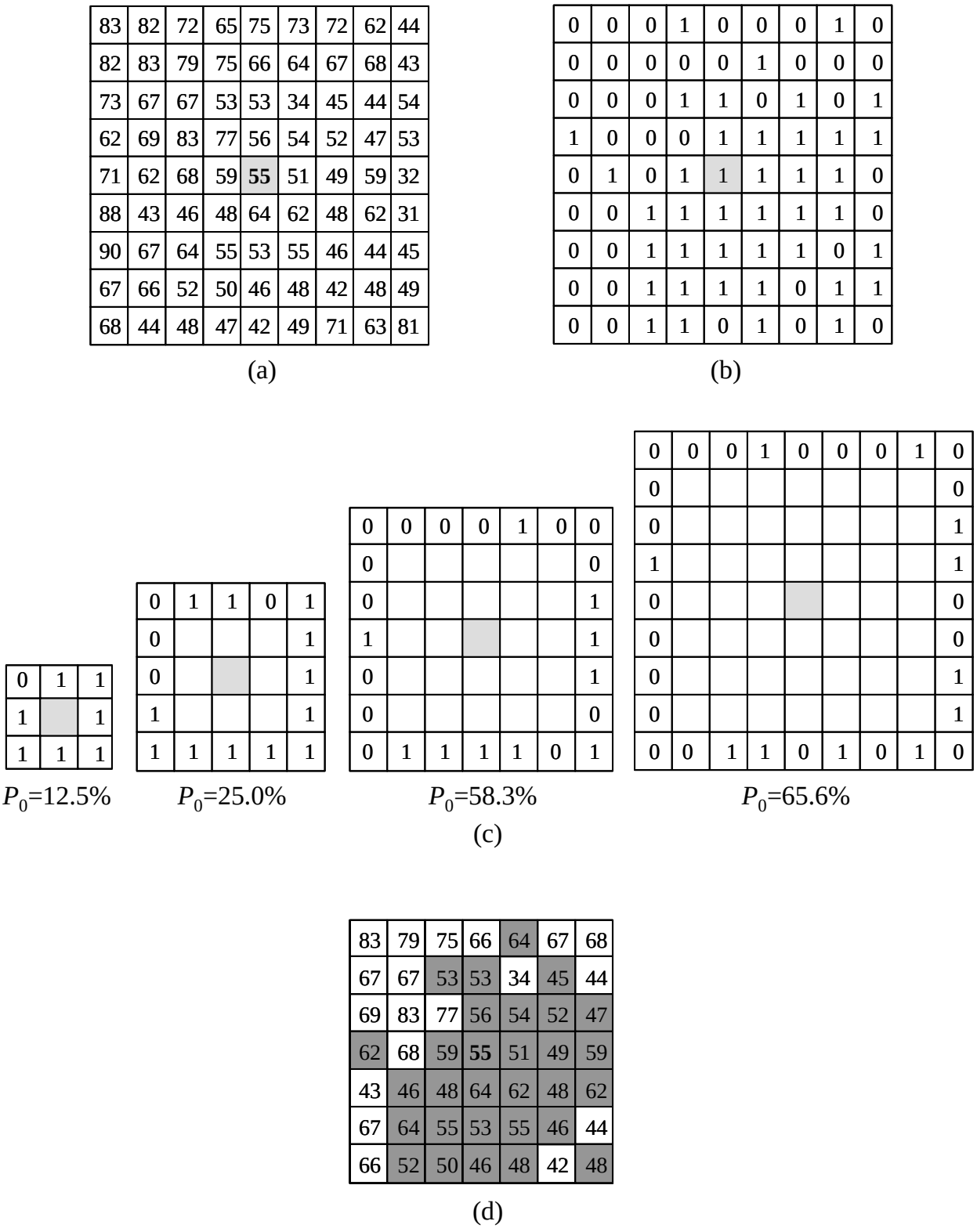

Fig.1 An example corresponding to each step of APMF procedure. (a) A window image (W_{max}=9) in Step 2. (b) Assigned mask image from (a) in case of T=10 in Step 3. (c) Calculation of the percentage of P_0 of external area at W=[3, 5, 7, 9] in Step 4. When P=60%, W=7 are determined as actual window size. (d) Median value obtained from pixel values (in dark gray pixels) corresponding with mask value 1 in the mask image (W=7) replaces the center pixel value [$I(i_c, j_c)$=55 changes to $I(i_c, j_c)$=53].

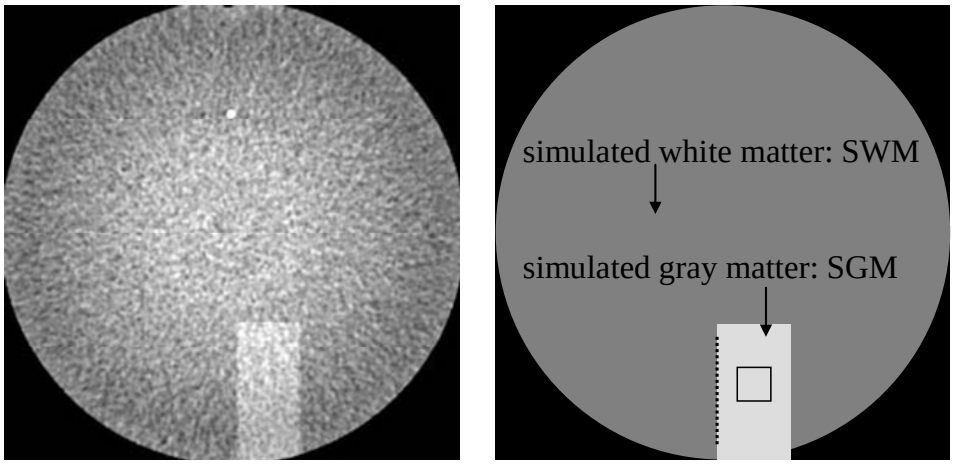

Fig.2 A simulation image (left: 400mAs, 6HU) and its sketch (right). Dotted line in the sketch suggests a vertical edge line of 80 pixels length for *ESR* calculation. Its horizontal coordinate value is C_x. Square in the sketch suggests a region for *SDR* calculation. Its size is 20×20 pixels.

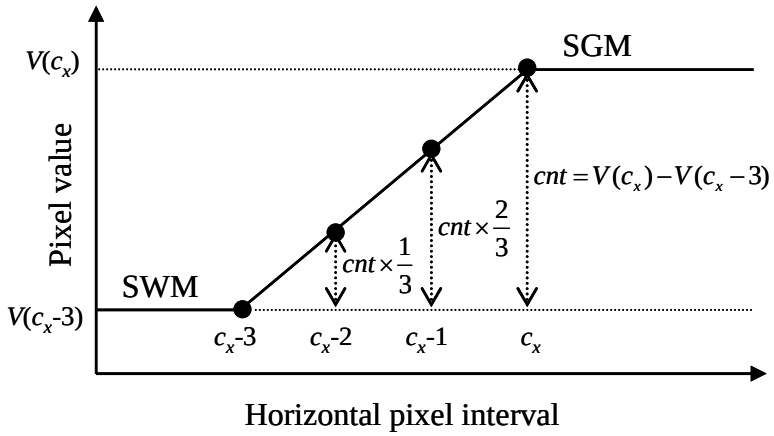

Fig.3 An explanatory diagram with regard to edge slope of SGM-SWM interface.

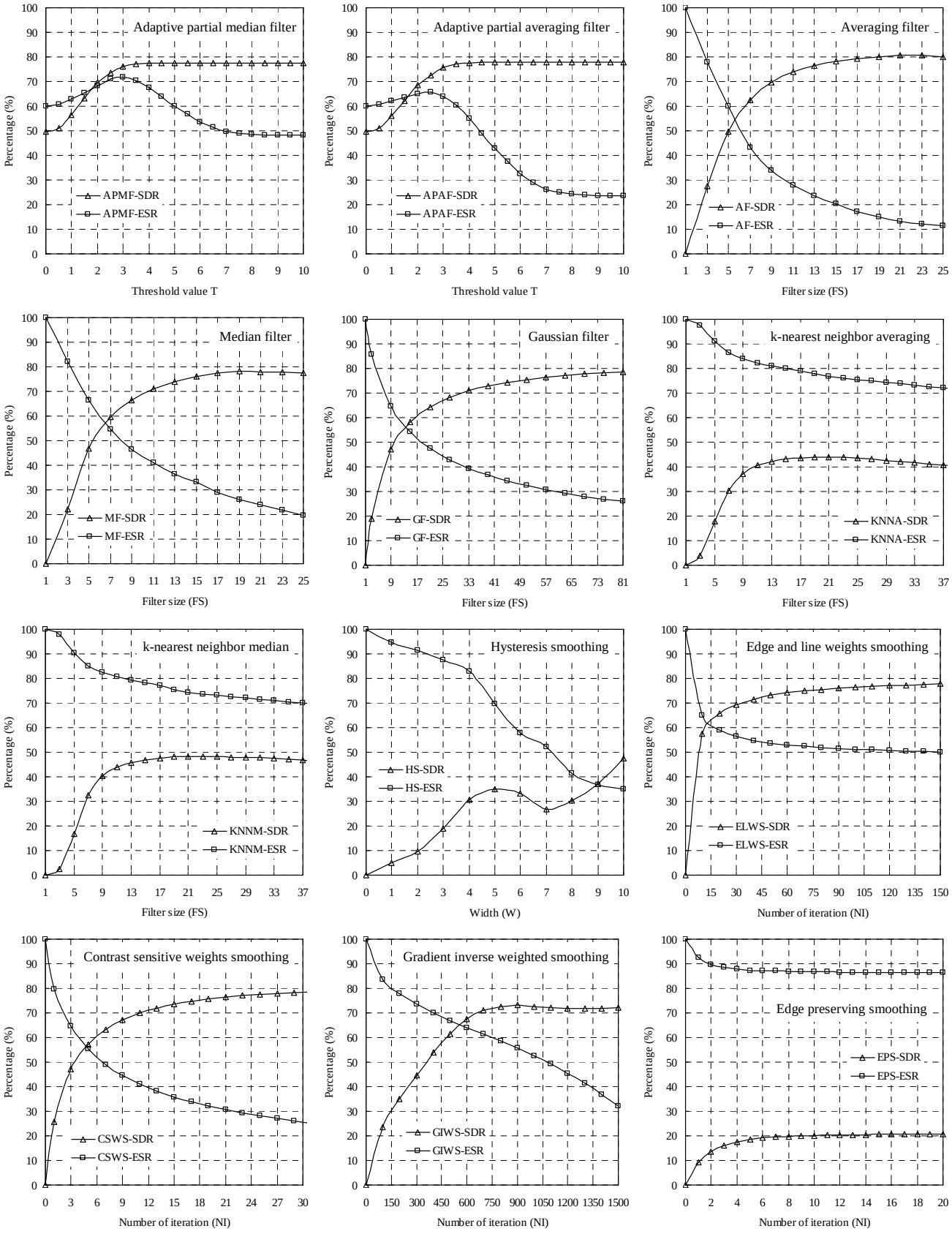

A part of Fig.4

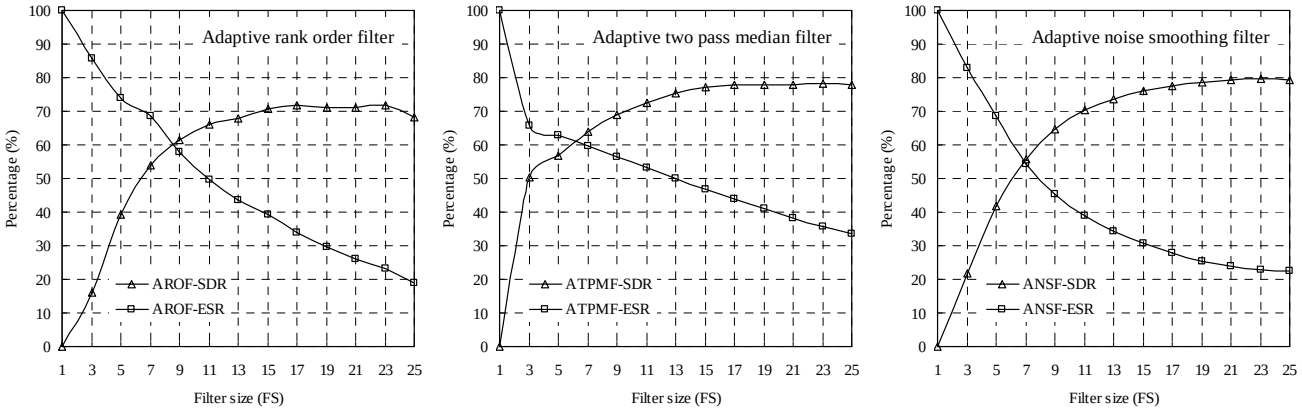

Fig.4 Graphs of SDR and ESR obtained from simulation images in condition of 400mAs, 6HU.

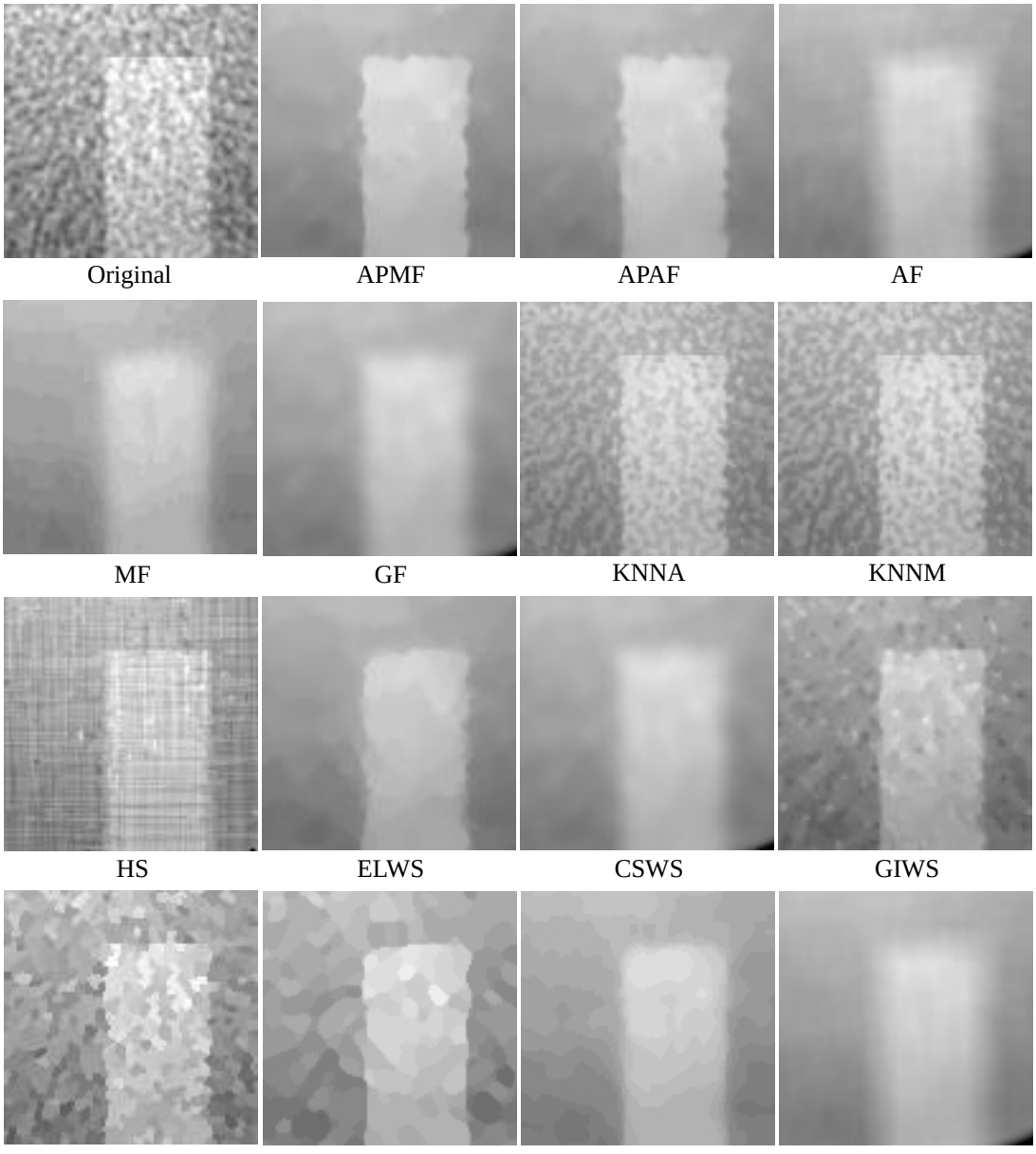

Fig.5 Various processed images (400mAs, 6HU) with parameters in Table 1.

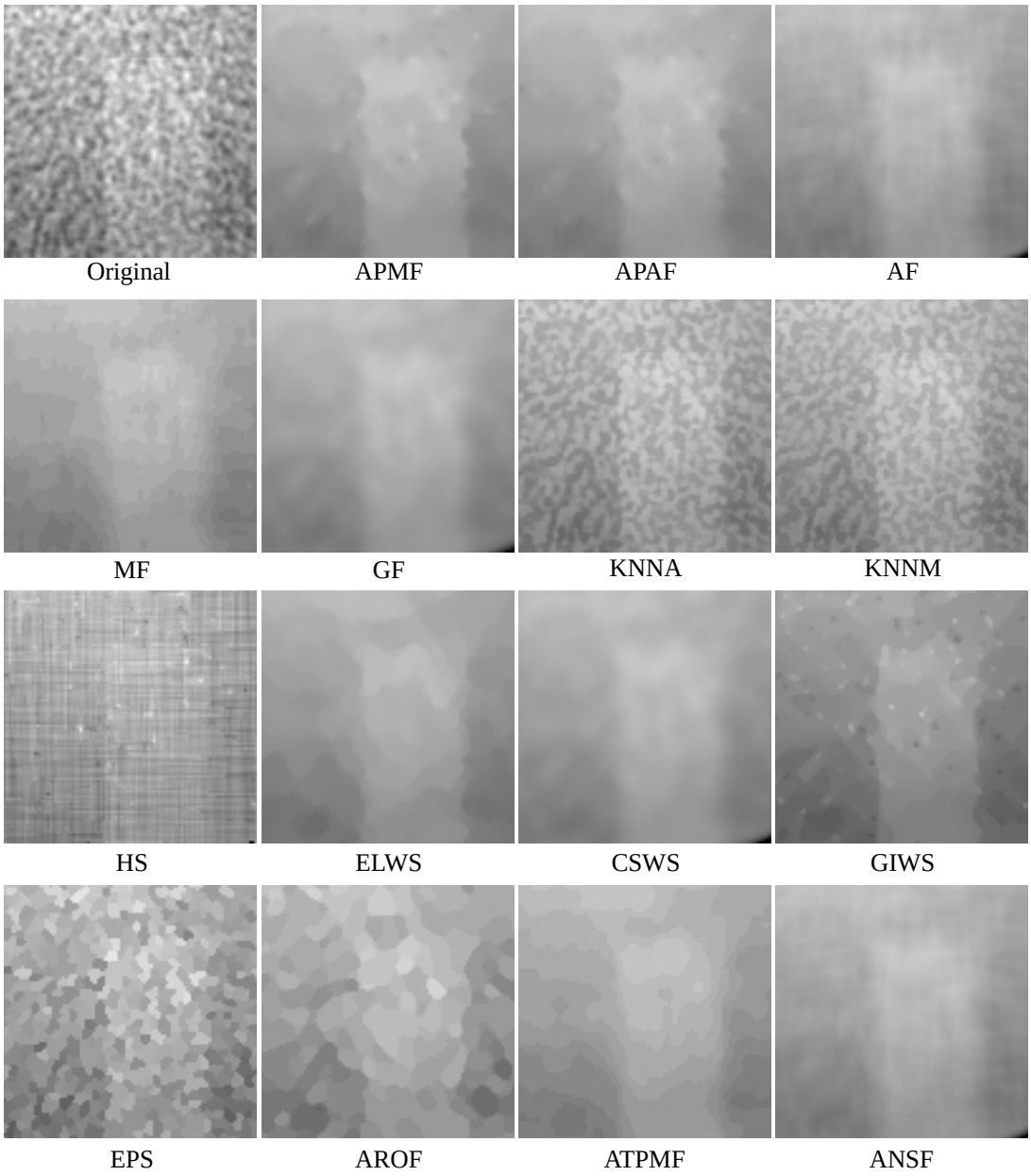

Fig.6 Various processed images (400mAs, 3HU) corresponding to either SDR≈75% or ESR≈49%. These numerical values were obtained from APMF images.

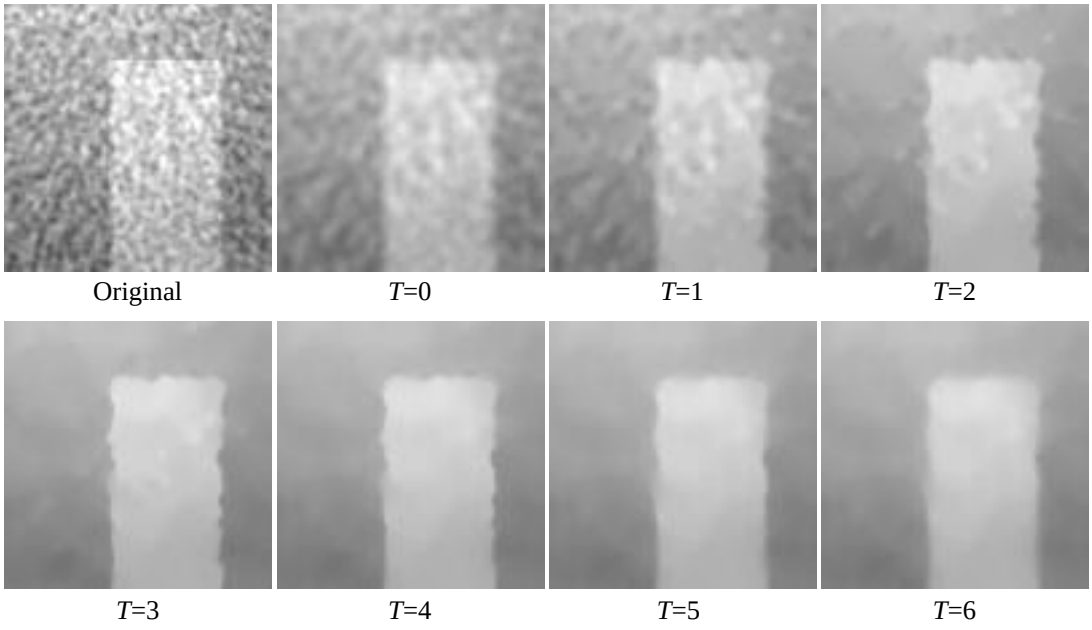

Fig.7 APMF processed images (400mAs, 6HU) by varying T.

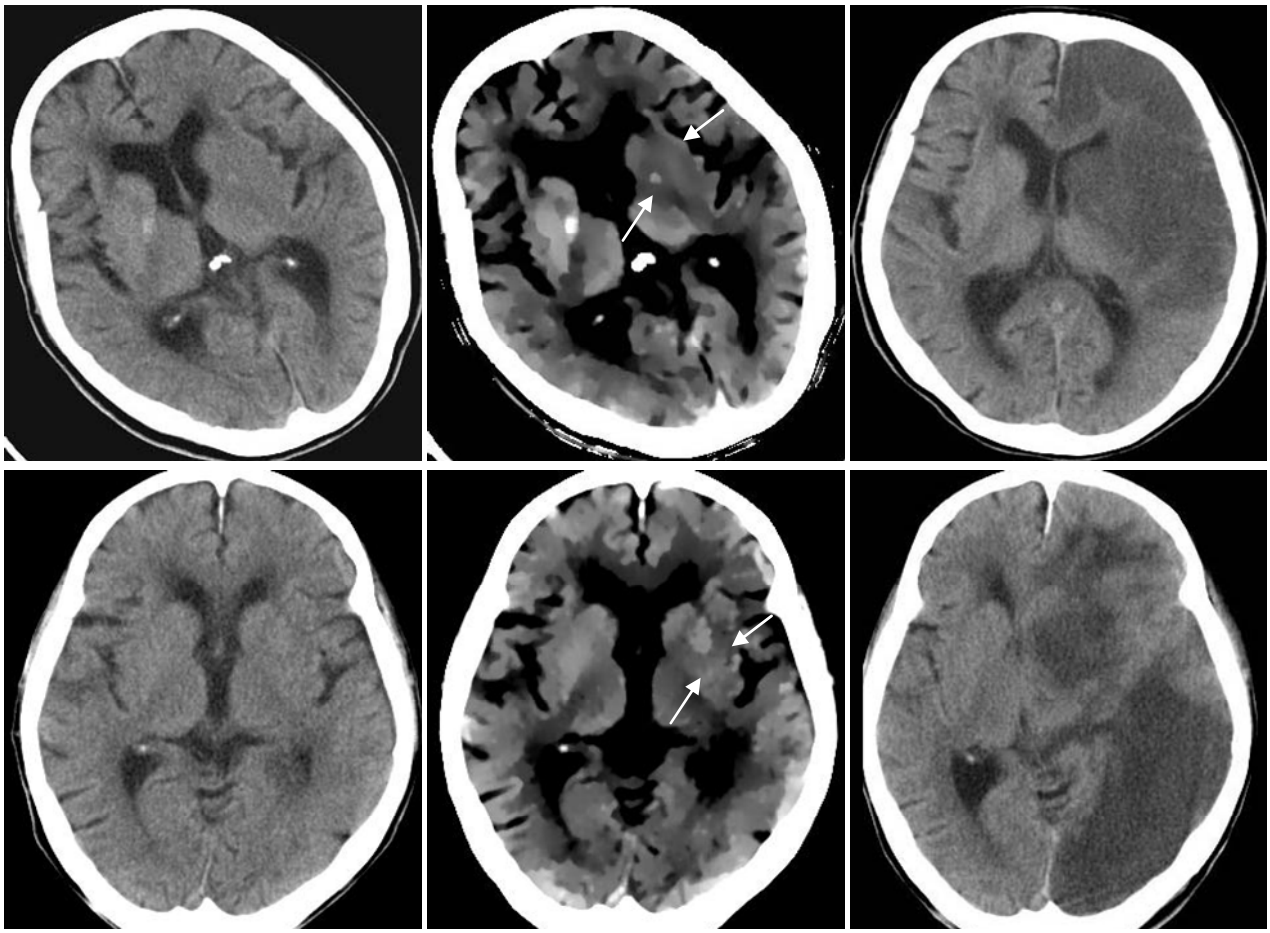

Fig.8 Two examples of abnormal cases. Lefts are original images (WL=35, WW=80). Middles are APMF images (WL=35, WW=20). Rights are follow-up images obtained several days after the onset of symptoms (WL=35, WW=80). Arrows indicate obscuration of the lentiform nucleus.

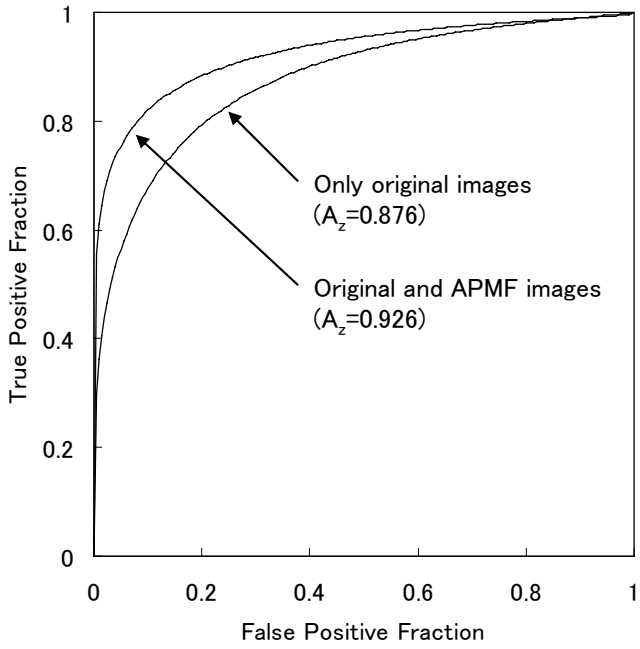

Fig.9 Average ROC curves of four radiologists for diagnosis of acute stroke from brain CT images without the APMF images and with the APMF images.

Table 1 A list of compared methods and comparison results.

Method	Parameters	SDR(%)	ESR(%)
Adaptive partial median filter (APMF)	M=5, Wmax=13, P=60, T=3	76.0	71.7
Adaptive partial averaging filter (APAF) [16],[17]	M=5, Wmax=13, P=60, T=3	75.6	64.0
Averaging filter (AF) [18]	FS=13	76.4	23.6
Median filter (MF) [19]	FS=15	76.1	33.1
Gaussian filter (GF) [18]	FS=55, σ=(FS-1)/4	76.1	31.2
Adaptive two pass median filter (ATPMF) [27]	FS=13, a =1, b =1	75.4	49.9
Adaptive noise smoothing filter (ANSF) [28]	FS=15	76.0	30.6
Edge and line weights smoothing (ELWS) [23]	NI=93	76.0	51.4
Contrast sensitive weights smoothing (CSWS) [23]	NI=20, σ=50	76.0	31.3
Hysteresis smoothing (HS) [22]	Width=5	35.0	69.7
k-nearest neighbor averaging (KNNA) [20]	FS=37, k=FS×FS/2	40.7	72.0
k-nearest neighbor median (KNNM) [21]	FS=31, k=FS×FS/2	47.9	71.5
Adaptive rank order filter (AROF) [26]	FS=7, k=eq.(6) in [26]	54.0	68.7
Gradient inverse weighted smoothing (GIWS) [24]	NI=352	49.5	71.7
Edge preserving smoothing (EPS) [25]	NI=10	20.1	86.7

Table 2 A_z values for each observer.

Observer	A_z value	
	Only original images	Original + APMF images
A	0.912	0.952
B	0.881	0.922
C (resident)	0.842	0.914
D (resident)	0.866	0.916
Mean	0.876	0.926

Note.-The difference was statistically significant with a *P* value of 0.04.